

See discussions, stats, and author profiles for this publication at: <https://www.researchgate.net/publication/260004570>

Ambient Surface Analysis of Organic Monolayers using Direct Analysis in Real Time Orbitrap Mass Spectrometry

ARTICLE in ANALYTICAL CHEMISTRY · JANUARY 2014

Impact Factor: 5.64 · DOI: 10.1021/ac4031626 · Source: PubMed

CITATIONS

4

READS

64

14 AUTHORS, INCLUDING:



Aline Debrassi

Surflay Nanotec GmbH

19 PUBLICATIONS 162 CITATIONS

SEE PROFILE



Nagendra Bhairamadgi

Wageningen University

12 PUBLICATIONS 76 CITATIONS

SEE PROFILE



Luc Scheres

Wageningen University

30 PUBLICATIONS 618 CITATIONS

SEE PROFILE



Karin Schroën

Wageningen University

84 PUBLICATIONS 1,257 CITATIONS

SEE PROFILE

Ambient Surface Analysis of Organic Monolayers using Direct Analysis in Real Time Orbitrap Mass Spectrometry

Radostina K. Manova,[†] Sweccha Joshi,[†] Aline Debrassi,[†] Nagendra S. Bhairamadgi,[†] Esther Roeven,^{||} Jacinthe Gagnon,[†] Muhammad N. Tahir,[†] Frank W. Claassen,[†] Luc M.W. Scheres,^{||} Tom Wennekes,[†] Karin Schroën,[‡] Teris A. van Beek,^{*,†} Han Zuilhof,[†] and Michel W. F. Nielen[†]

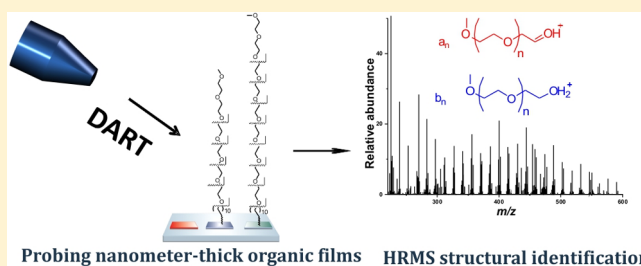
[†]Laboratory of Organic Chemistry, Wageningen University, Dreijenplein 8, 6703 HB Wageningen, The Netherlands

[‡]Food Process Engineering Group, Wageningen University, Bomenweg 2, 6703 HD Wageningen, The Netherlands

^{||}Surfix BV, Dreijenplein 8, 6703 HB Wageningen, The Netherlands

Supporting Information

ABSTRACT: A better characterization of nanometer-thick organic layers (monolayers) as used for engineering surface properties, biosensing, nanomedicine, and smart materials will widen their application. The aim of this study was to develop direct analysis in real time high-resolution mass spectrometry (DART-HRMS) into a new and complementary analytical tool for characterizing organic monolayers. To assess the scope and formulate general interpretation rules, DART-HRMS was used to analyze a diverse set of monolayers having different chemistries (amides, esters, amines, acids, alcohols, alkanes, ethers, thioethers, polymers, sugars) on five different substrates (Si, Si₃N₄, glass, Al₂O₃, Au). The substrate did not play a major role except in the case of gold, for which breaking of the weak Au–S bond that tethers the monolayer to the surface, was observed. For monolayers with stronger covalent interfacial bonds, fragmentation around terminal groups was found. For ester and amide-terminated monolayers, in situ hydrolysis during DART resulted in the detection of ions characteristic of the terminal groups (alcohol, amine, carboxylic acid). For ether and thioether-terminated layers, scission of C–O or C–S bonds also led to the release of the terminal part of the monolayer in a predictable manner. Only the spectra of alkane monolayers could not be interpreted. DART-HRMS allowed for the analysis of and distinction between monolayers containing biologically relevant mono or disaccharides. Overall, DART-HRMS is a promising surface analysis technique that combines detailed structural information on nanomaterials and ultrathin films with fast analyses under ambient conditions.



Probing nanometer-thick organic films HRMS structural identification

Nanomaterials, for example, monolayers, nanoparticles, quantum dots, stimuli-responsive polymers, and smart materials, are rapidly commercialized, for example, in nanomedicine, electronics, biosensors, and over 60 nanomaterials are currently on the market.¹ Thus, nanomaterial characterization is needed for proper quality control, process efficiency,² and environmental health risk assessment.³ Nanofabrication of biosensors, often involves multiple surface modification steps⁴ of monolayers grafted on the sensor surface. A proper surface characterization of each modification step would assist the desired control at a molecular level.

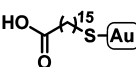
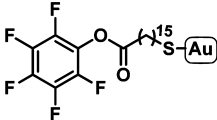
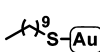
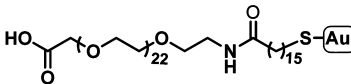
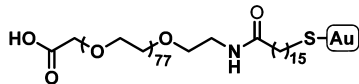
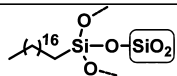
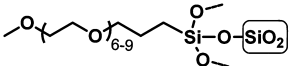
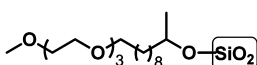
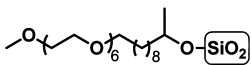
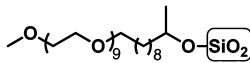
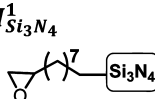
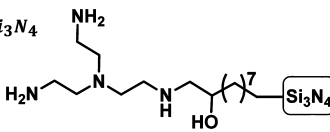
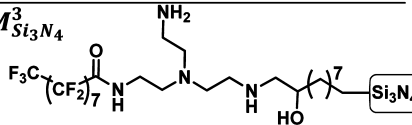
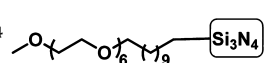
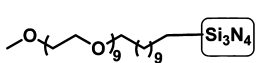
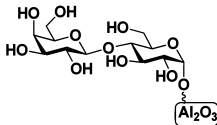
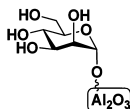
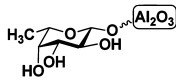
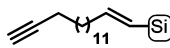
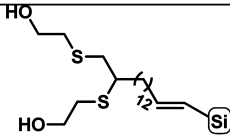
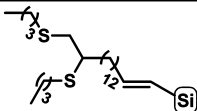
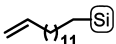
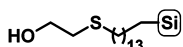
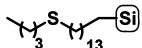
The most frequently used technique for surface analysis is X-ray photoelectron spectroscopy (XPS). XPS provides qualitative and quantitative information, yet suffers from a lack of chemical resolution. Surface mass spectrometry (MS) has, gained considerable attention as a complementary surface analysis technique.⁵ Secondary ion MS (TOF-SIMS) is the most common MS method for MS imaging of surfaces.^{6–10} The TOF-SIMS analysis of self-assembled monolayers (SAMs)^{9,11} on gold revealed, however, extensive fragmentation. This led to low secondary ion yields and a poor signal-to-noise ratio.

Alternative MS analytical techniques for SAMs are laser desorption MS (LDMS),^{12,15,16} thermodesorption high-resolution MS (TD-HRMS),¹³ two-laser MS (L2MS),^{9,14} and matrix-assisted laser desorption/ionization mass spectrometry MS (MALDI-MS).¹⁵ The latter is able to probe different surfaces, which recently opened up new perspectives in the molecular identification of SAMs,¹⁷ nanoparticles,¹⁸ biosensors,¹⁹ and biochips.²⁰ Actually, the combination of surface MALDI-MS and SAMs on gold evolved in a technique termed by Mrksich as SAMDI.²¹ Upon MALDI, the interfacial Au–S bond breaks and the resultant intact modified thiolate is released. So far, the SAMDI approach was not only applied to subsequent surface reactions, but also to study biochemical reactions on the interface of tailor-made monolayers,²² to perform immunoassays²³ or enzyme assays,²⁴ and to screen novel multicomponent reactions.²⁵ Unfortunately, the use of MALDI-MS is limited to the analysis of higher molecular

Received: October 2, 2013

Accepted: January 31, 2014

Table 1. Overview of Organic Monolayers Studied with DART-HRMS

Substrate	Symbol and the corresponding monolayer structure		
Au	M_{Au}^1 	M_{Au}^2 	M_{Au}^5 
	M_{Au}^3 	M_{Au}^4 	
SiO ₂	$M_{SiO_2}^1$ 	$M_{SiO_2}^2$ 	
	$M_{SiO_2}^{EO3}$ 	$M_{SiO_2}^{EO6}$ 	$M_{SiO_2}^{EO9}$ 
Si ₃ N ₄	$M_{Si_3N_4}^1$ 	$M_{Si_3N_4}^2$ 	$M_{Si_3N_4}^3$ 
	$M_{Si_3N_4}^{EO6}$ 	$M_{Si_3N_4}^{EO9}$ 	
Al ₂ O ₃	$M_{Al_2O_3}^{lac}$ 	$M_{Al_2O_3}^{man}$ 	$M_{Al_2O_3}^{fuc}$ 
Si	M_{Si}^1 	M_{Si}^2 	M_{Si}^3 
	M_{Si}^4 	M_{Si}^5 	M_{Si}^6 

weight (>300 Da) compounds because of MALDI matrix interferences and signal suppression.¹⁷ Moreover, the inhomogeneous distribution of matrix and the resulting poor shoot-to-shoot reproducibility,²⁶ as well as the choice of a suitable matrix for monolayer analysis²¹ are additional complicating factors.

To circumvent the aforementioned shortcomings, ambient MS has been considered as an alternative,²⁷ because it provides fast analysis and direct ionization of the sample without the need of sample preparation, addition of matrix, highly energetic ion beams, high vacuum, or laser irradiation. Moreover, the ambient ionization sources can be hyphenated with most types of atmospheric pressure ionization mass spectrometers.²⁷ So far ambient MS has been applied for SAMs on noble metal surfaces as gold²⁸ or copper.²⁹ In all cases, upon ambient plasma ionization, either with direct analysis in real time (DART)²⁸ or with low-temperature plasma (LTP),²⁹ the desorption of monomeric and dimeric thiolate molecules from the gold surfaces was observed, which is consistent with previous surface MS studies.^{9,13,14,17} However, little is known about the fragmentation of monolayers with stronger interfacial bonds tethering the monolayer, that is, covalently bound monolayers on glass,³⁰ silicon nitride (Si₃N₄),³¹ silicon (Si),³² alumina (Al₂O₃),³³ etc.

We showed previously that several ester and amide-terminated monolayers on Si₃N₄ could be analyzed by means

of DART-HRMS.³⁴ The sensitivity was in the picomole range, and the high selectivity of the mass spectrometer even allowed the structure elucidation of mixed monolayers, differing only by the type of halogen present, which was not possible with, for example, XPS. Although this seemed promising, only one substrate and only two functional groups were investigated. Thus, the general usefulness of DART-MS as a surface analysis tool was not assessed.

Here, we aim to develop DART-HRMS into a widely applicable analytical surface tool. To this end, a wide variety of monolayers, with different head and tail groups, were grafted onto gold, silicon nitride, silicon, glass, and alumina surfaces. The monolayers were modified employing various surface reactions: click reactions (i.e., thiol-ene, thiol-yne, and copper-catalyzed cycloaddition reactions), esterification, and amidation. The resulting modified surfaces were investigated by XPS and DART-HRMS, and their mass spectra were analyzed to arrive at a set of interpretation rules to deduce the surface chemistry present. Finally, three commercially available monolayers were studied to evaluate the usefulness for quality control.

EXPERIMENTAL SECTION

All chemicals, solvents, inorganic substrates, commercially available coatings, the synthesis of azidoundecanyl carbohydrates (1, 4, and 7), and the preparation of the monolayers are

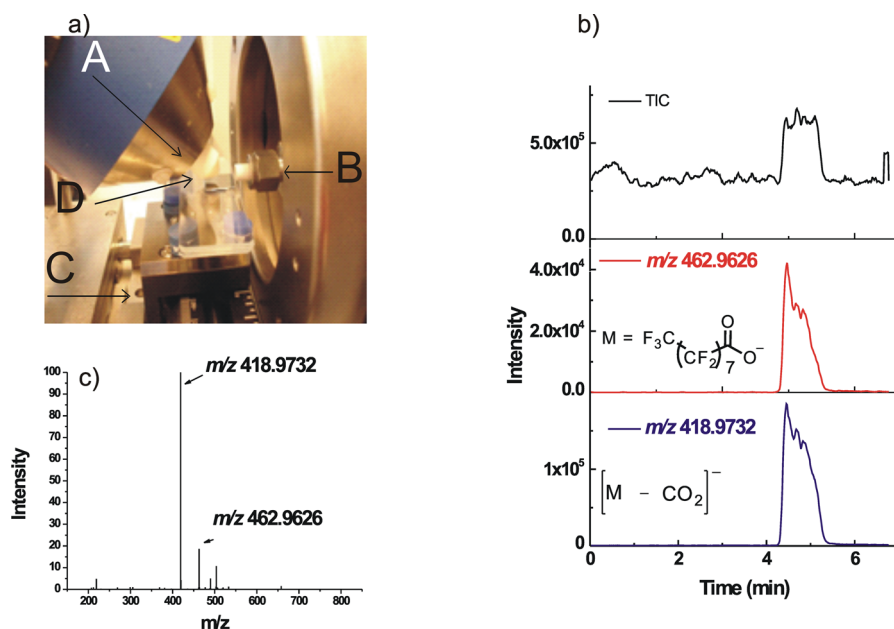


Figure 1. (a) DART-HRMS experimental setup used for the characterization of organic monolayers. (A) DART source pointed at 45° toward the sample. For a video of an actual measurement, see the SI. (B) MS inlet. (C) Motorized rail. (D) 1×1 cm Si_3N_4 sample. (b) DART-HRMS of the reversed amide monolayer $\text{M}_{\text{Si}_3\text{N}_4}^3$ in negative-ion mode, measured between 4.2 and 5.3 min. From top to bottom: Total ion current (TIC), the extracted ion current (EIC) of $\text{CF}_3(\text{CF}_2)_7\text{COO}^-$ at m/z 462.9626 and EIC of $\text{CF}_3(\text{CF}_2)_7^-$ at m/z 418.9732. (c) Mass spectrum of monolayer $\text{M}_{\text{Si}_3\text{N}_4}^3$.

described in the Supporting Information (SI). Monolayers, investigated in this study, are depicted in Table 1.

X-ray Photoelectron Spectroscopy (XPS). Each monolayer formation was first confirmed by XPS. Prior to analysis, all substrates were extensively cleaned by sonication in appropriate solvents and dried under a stream of argon (for details see SI). XPS analyses were performed as described elsewhere.³⁵

Direct Analysis in Real Time High-Resolution Mass Spectrometry (DART-HRMS). The DART-HRMS system consisted of a DART-SVP (IonSense, Saugus, U.S.A.) coupled to an Exactive Orbitrap high-resolution mass spectrometer (HRMS) (Thermo Fisher Scientific, San Jose, CA, U.S.A.). The MS was daily calibrated. The resolution was set at “ultrahigh” (100 000 fwhm at m/z 200 at a scan rate of 1 Hz). The mass range was either m/z 50–300 or 100–2000. Xcalibur software (version 2.1) was used for instrument control, data acquisition and data processing. Ions with values within ± 1.5 mDa of the theoretical values were considered in the structural elucidation of organic monolayers. The ionizing gas of DART was He with a fixed flow of ~ 3.5 L/min and the temperature set at 450°C . DART settings in positive-ion mode and in negative-ion mode were as described previously.³⁴ The actual temperature of 199°C in the ionization region at the surface of the specimen was measured with a Testo surface temperature sensor (Distrelec B.V, Utrecht, Netherlands) in static mode.

Specimens. Modified monolayer samples (0.7×1.5 cm or 1×1 cm), together with a nonmodified, freshly cleaned sample, were immobilized on a glass slide (Figure 1a). The glass slide with the specimens was carefully positioned on top of the motorized rail. The motorized rail moves horizontally and was used to introduce samples in and out of the ionization region (region between DART outlet and MS inlet). The DART outlet was pointed at an angle 45° to the sample and the height adjusted to minimize the DART outlet–sample distance, while still avoiding direct contact (typically ~ 1 cm). After optimization of the sample stage, the samples were removed

from the ionization region via the rail and the DART heating was started. When the DART temperature reached the set value, the samples were moved slowly (0.2 mm/s) toward the ionization region. Meanwhile the acquisition of data was started and in this way, ions from the ambient atmosphere, from the glass slide, and the nonmodified sample were also collected and used for comparison and background subtraction. For collecting spectra in positive and negative-ion mode individual specimens were used. The obtained mass spectra and video material of a measurement can be found in the Supporting Information (SI).

RESULTS AND DISCUSSION

DART-HRMS of Amide and Ester-Terminated Monolayers. First, samples were analyzed that could clarify the role of hydrolysis in ester and amide-functionalized monolayers. We reported previously³⁴ that ester-containing monolayers on Si_3N_4 could be identified in negative-ion mode by ions related to the free alcohol. Similarly, in positive-ion mode, amide monolayers were characterized by ions associated with the free amine. In both cases, the alcohol or amine had reacted with the activated terminal carboxylic acid moiety of an already present monolayer on Si_3N_4 ($\text{ROC}(=\text{O})(\text{CH}_2)_{10}-\text{Si}_3\text{N}_4$ and $\text{RNHC}(=\text{O})(\text{CH}_2)_{10}-\text{Si}_3\text{N}_4$, respectively). On the basis of these findings, we hypothesized that in situ hydrolysis occurred during DART ionization with (protonated) water molecules, involved in the ionization process,³⁶ giving rise to the release of the free alcohol or amine. To test this hypothesis, the reversed amide $\text{M}_{\text{Si}_3\text{N}_4}^3(\text{CF}_3(\text{CF}_2)_7\text{C}(=\text{O})\text{NH}-\text{R}-\text{Si}_3\text{N}_4)$ was constructed by reacting a carboxylic acid with a terminal amine group of a monolayer on Si_3N_4 . If in situ hydrolysis with or without simultaneous ionization proceeds during DART, then reverse amide monolayer $\text{M}_{\text{Si}_3\text{N}_4}^3$ (Table 1) should yield ions of the corresponding carboxylate component.

In the top panel of Figure 1b, the total ion current of $M_{Si_3N_4}^3$ shows when the sample is moved under the DART beam (between 4.2 and 5.3 min). The spectrum in this interval revealed the ions $CF_3(CF_2)_7COO^-$ at m/z 462.9626 (middle panel) and $CF_3(CF_2)_7^-$ at m/z 418.9732 (bottom panel), as base peak (Figure 1c). This indicates that amide hydrolysis is indeed the dominant process.

To confirm that hydrolysis is not influenced by the substrate, we compared the negative-ion mode spectrum of the previously reported³⁴ pentafluorophenyl ester-terminated monolayer on Si_3N_4 , $C_6F_5OC(=O)(CH_2)_{10}-Si_3N_4$, with that of a pentafluorophenyl ester-terminated monolayer on Au, $C_6F_5OC(=O)(CH_2)_{14}CH_2S-Au$ (Table 1, M_{Au}^2). For both monolayers, the ion $[C_6F_5O]^-$ that results from ester hydrolysis, was observed at m/z 182.9860. Therefore, the substrate linkage appears of only minor importance in effecting the formation of hydrolysis products.

DART-HRMS of Monolayers Having S–Au Bonds.

DART-MS should be able to reveal information on the strength of the interfacial bond tethering the monolayer. To this aim, we continued to investigate ester-terminated monolayers, but now in positive-ion mode. No fragments associated with the carboxylate function of the $C_6F_5OC(=O)(CH_2)_{10}-Si_3N_4$ were detected, while the analysis of $C_6F_5OC(=O)(CH_2)_{15}S-Au$ (M_{Au}^2) revealed the presence of the ion $[C_6F_5OC(=O)(CH_2)_{15}-S]^+$ at m/z 453.1870 (see mass spectral library, SI Figure S5). Apparently, while the Si–C and N–C bonds do not easily break under these conditions, the weak Met–S bond (Met = Au, Cu) is preferentially cleaved, resulting in the formation of positive ions containing the whole monomer of the SAMs, a finding that corroborates other surface MS studies on S–Au monolayers.^{28,29} In this regard, the substrate plays a role in the fragmentation of the monolayer, especially when the interfacial bond is weak enough to break and yields stable ions of sufficient volatility.

Next monolayers lacking hydrolyzable bonds, for example, the SAMs $HOOC(CH_2)_{14}CH_2S-Au$ (Table 1, M_{Au}^1), and $CH_3(CH_2)_9S-Au$ (Table 1, M_{Au}^5) were studied. They were first analyzed in positive-ion mode, because under these conditions desorption of intact ions from the noble metal surface are most likely to be observed.^{14,28,29} In positive-ion mode $CH_3(CH_2)_9S-Au$, did not show the ions $[CH_3(CH_2)_9S]^+$ and the corresponding dimers $[CH_3(CH_2)_9S-SH-(CH_2)_9CH_3]^+$. Instead, many oxidation products were observed: $[M + 2O - H]^+$, $[M + O - 3H]^+$, $[M + O - H]^+$, $[M + 3O - H]^+$, and $[M + 2O - 3H]^+$ for the monomeric molecules (Figure 2, upper panel) and $[2M - SH + 2O]^+$, $[2M - SH + 2O - H_2O]^+$, and $[2M - H_2S + 5O]^+$ for the dimers (Figure 2, middle panel), where M is $CH_3(CH_2)_9SH$. Combined, the ions provide proof for the presence of decanethiol. In the m/z 170–220 mass range, several ions unrelated to the monolayer were observed, which shows the necessity of carrying out scans of nonmodified substrate, that is, in this case gold. The ions at m/z 206, 207, 328, and 380 were related to the monolayer but could not be assigned.

In negative-ion mode, the spectrum of $CH_3(CH_2)_9S-Au$ (M_{Au}^5) revealed two oxidation products of decanethiol also present in positive-ion mode but now negatively charged, that is, $[M + 3O - H]^-$ and $[M + 2O - H]^-$, as well as $[M + 2O - H_2S - H]^-$ at m/z 171.1382 (Figure 2, lower panel). Thus the positive-ion mode measurements corroborated the negative-ion conclusions. The presence of extensive oxidation in both

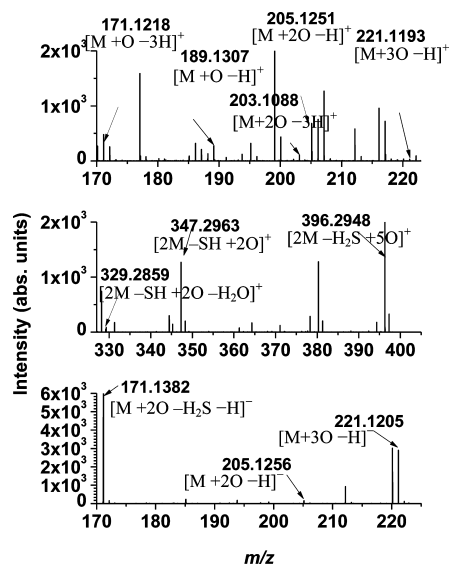


Figure 2. DART-HRMS of M_{Au}^5 (decanethiol on gold) in positive (m/z 170–220, upper; m/z 325–405, middle) and negative-ion mode (m/z 170–225, lower), providing similar information. The ions at m/z 177, 199, 212, 216, and 217 in positive-ion mode are due to background.

negative and positive-ion modes can be explained by the close proximity of the DART outlet to the MS inlet and the specimen. Under such geometric conditions, the presence of a relative high abundance of reactive $O_2^{+•}$ species has been reported.³⁶ Alkylsulfonate anions are also prominently present in negative ion spectra obtained with TOF-SIMS¹¹ or LDMS¹² of different sulfur-containing monolayers. However, other thiol molecular species such as $[M - H]^+$, $[M - H]^-$ and dimeric molecular species such as $Met[M - H]_x^-$ (Met = Au, Ag, Cu, Pt; M = thiol; $x = 2-4$) are the most characteristic ions in TOF-SIMS spectra,^{10,37,38} while DART ionization mainly produced oxidation products. Positive secondary ion mass spectra obtained with TOF-SIMS¹⁰ are, on the other hand, dominated by ions characteristic of long-chain hydrocarbons, namely C_xH_y , and a variety of fragments originating from the alkyl chain. These ions were absent in the DART-HRMS spectra of M_{Au}^5 , that is, such extensive fragmentation was not observed.

The SAM M_{Au}^1 demonstrated the formation of sulfonium ions $[HOOC-(CH_2)_{15}-S]^+$ at m/z 287.2034. In its spectrum, the ions corresponding to the loss of water at m/z 269.1931 and to the loss of H_2 at m/z 285.1878 were even more intense (mass spectral library, Figure 4). Additionally, the ion related to the loss of H_2S at m/z 253.2159 was detected. Interestingly, the above-mentioned cations were scarcely present in the spectrum of the solution of the free thiol $HS-(CH_2)_{15}-COOH$ or when present on a glass surface. Instead, the ammonia adduct $[HS-(CH_2)_{15}-COOH + NH_4]^+$ was predominantly formed together with the ion for $[HS-(CH_2)_{15}-COOH + NH_4 + H_2O - NH_3]^+$. In other words, DART-HRMS analysis was able to discriminate between covalently bound thiolates on flat gold surfaces and unbound thiol molecules on glass.

DART-HRMS of Monolayers Having C–S Bonds.

Considering this, monolayers with C–S bonds were also probed in order to test whether stronger covalent bonds could be cleaved, giving rise to characteristic fragments. To this aim, two different thiols, i.e. mercaptoethanol and butanethiol, were covalently attached to an alkyne (Table 1, M_{Si}^1) and an alkene

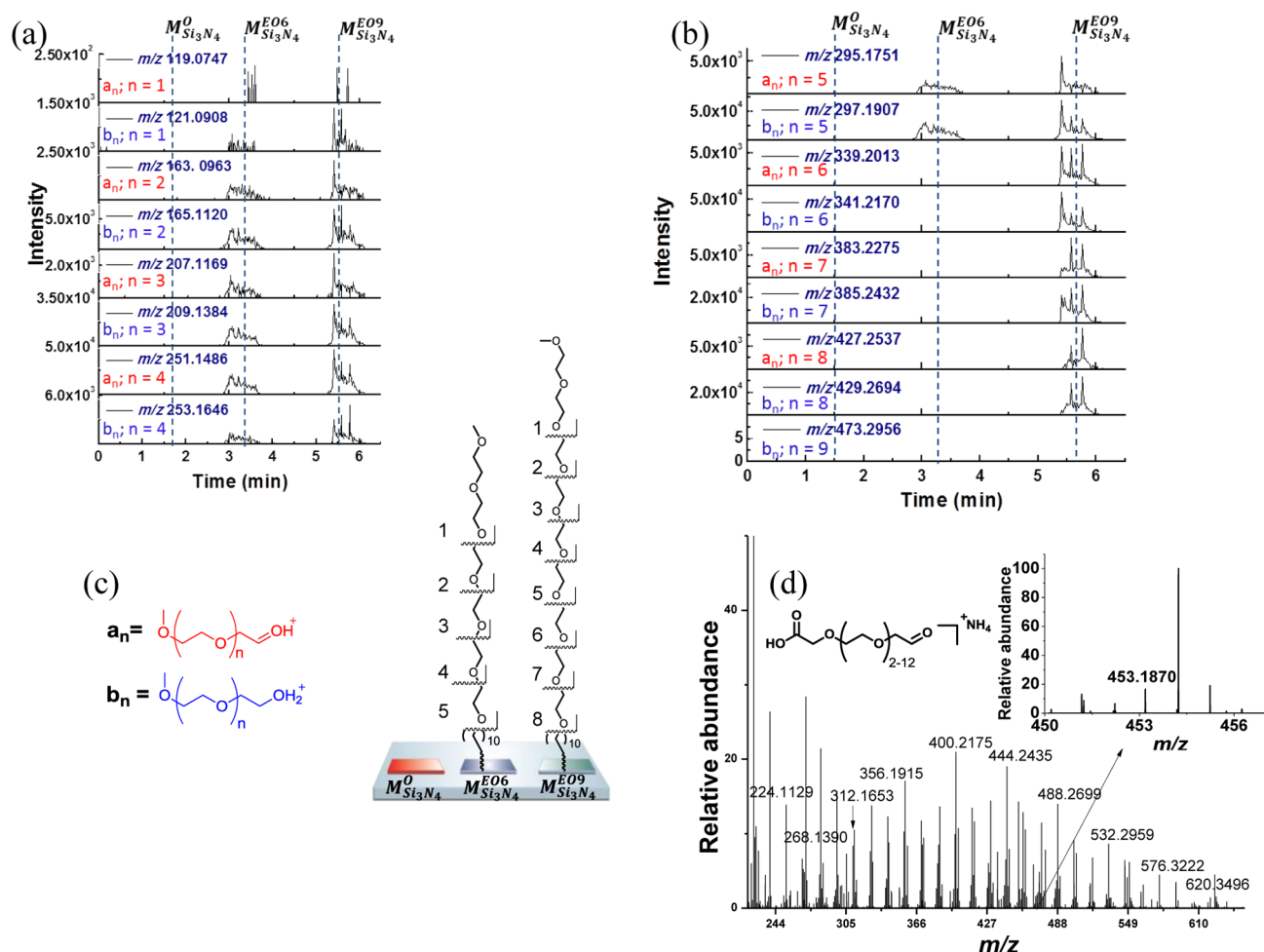


Figure 3. (a and b) Reconstructed ion chronograms in positive-ion mode of $M_{Si_3N_4}^0$ (a nonmodified Si_3N_4 substrate, measured between 1.0 and 2.0 min) and methoxy-oligo(EO) monolayers $M_{Si_3N_4}^{EO6}$ (3.0–4.0 min) and $M_{Si_3N_4}^{EO9}$ (5.2–6.2 min), showing in panel a ions from homologous series a_n and b_n with $n = 1–4$ and in panel b ions from homologous series a_n and b_n with $n = 5–9$. (c) Schematic representations of $M_{Si_3N_4}^0$, $M_{Si_3N_4}^{EO6}$, $M_{Si_3N_4}^{EO9}$, and structure of ions from homologous series a_n and b_n . (d) Positive-ion DART mass spectrum of carboxymethyl–PEG monolayer on gold (M_{Au}^3). The insert shows the ion at m/z 453.1870 $[C_6F_5OC(=O)(CH_2)_{15}-S]^+$ in positive-ion mode corresponding with remaining unreacted PFP moieties.

(Table 1, M_{Si}^4) monolayer on Si via thiol-yne or thiol-ene click reactions, respectively.³⁹ Thus, four different monolayers were obtained. Dithioether-terminated monolayer M_{Si}^2 and monothioether-terminated monolayer M_{Si}^5 , obtained via attachment of mercaptoethanol, have the same terminal groups but differ by their surface coverage of the attached mercaptoethanol in favor of M_{Si}^2 ($M_{Si}^2 > M_{Si}^5$; Table 1).³⁹ Similarly, monolayers M_{Si}^3 and M_{Si}^6 , obtained by attachment of butanethiol, have the same terminal groups but differ by their coverage ($M_{Si}^3 > M_{Si}^6$; Table 1). In contrast to the S–Au monolayers, DART-HRMS analysis of M_{Si}^2 , M_{Si}^3 , M_{Si}^5 , and M_{Si}^6 , in positive-ion mode gave no characteristic peaks, confirming the results obtained on Si_3N_4 that intact monolayers cannot be analyzed because of the strong interfacial bond. Negative-ion analysis, however, revealed ions related to oxidized mercaptoethanol. The monolayers M_{Si}^2 and M_{Si}^5 , for instance, were identified by the ions $[HO-(CH_2)_2SO_2]^-$ at m/z 108.9954 and $[HO(CH_2)_2SO_3]^-$ at m/z 124.9903 (mass spectral library, SI Figures S8 and S9). Likewise, monolayers M_{Si}^3 and M_{Si}^6 released the ion $[CH_3(CH_2)_3SO_3]^-$ at m/z 137.0268 (mass spectral library, SI Figures S10 and S11). The ion for $[CH_3(CH_2)_3SO_2]^-$ was not detected due to the presence of interfering background ions at m/z 121.0286. These results suggest that upon DART

ionization C–S bonds were cleaved, which broadens the scope of the application of this surface MS technique. Furthermore, two specimens of equal size, having the same thioether groups but with a different density (M_{Si}^3 and M_{Si}^5) were measured consecutively, and the intensity of the ions $[HO(CH_2)_2SO_2]^-$ and $[HO(CH_2)_2SO_3]^-$ on both monolayers was compared. Due to the different relative surface coverage,³⁹ it was observed that these ions were of approximately 1 order of magnitude higher intensity for M_{Si}^2 (dithioether-terminated monolayer) than for monolayer M_{Si}^5 (monothioether-terminated). Thus, on a relative basis, DART-MS can yield information on the surface coverage of similar monolayers.

DART-HRMS of Alkyl-Terminated Monolayers. Monolayers having a hydrocarbon chain e.g. the alkyne (C_{16}) M_{Si}^1 and alkene (C_{14})-terminated monolayer M_{Si}^4 on Si, and the epoxy-terminated monolayer $M_{Si_3N_4}^1$ on Si_3N_4 , showed neither in positive nor in negative-ion mode distinguishable fragmentation upon DART ionization. For instance, no peaks representing ions reported for n -alkanes³⁶ as $[C_nH_{2n+2} - H]^+$ and $[C_nH_{2n-1}]^+$ or their oxidation products were detected in positive-ion mode. The monolayer $M_{SiO_2}^3$, prepared via silane modification of glass and yielding a C_{18} -terminated monolayer,

demonstrated in negative-ion mode several distinguishable but unexplainable ions besides ions that were also detected on a clean nonmodified substrate. Recently, it was shown that only alkanes, significantly larger than C_{18} , can be ionized by DART in negative-ion mode, albeit with relatively poor sensitivity.⁴⁰ In addition, those alkanes were analyzable as $[M + O_2]^{-\bullet}$, and no extensive fragmentation was observed. Taking this into consideration, it is not surprising that the aforementioned alkyl-terminated monolayers were not identifiable with DART. In this respect, TOF-SIMS outperformed DART-HRMS with the ability to characterize alkyl-terminated monolayers because of the extensive formation of both organic and mixed organic/inorganic fragments from a variety of substrates including glass, silicon, and gold.^{37,41,42}

DART-HRMS of Oligo(Ethylene Glycol)-Terminated Monolayers. Whether DART-HRMS is applicable for identification of polyether monolayers, which are frequently applied to minimize biofouling, was addressed by analysis of monolayers $M_{SiO_2}^{EO3}$, $M_{SiO_2}^{EO6}$, $M_{SiO_2}^{EO9}$, $M_{Si_3N_4}^{EO6}$, and $M_{Si_3N_4}^{EO9}$. These methoxy-oligo(ethylene oxide) (EO)-terminated monolayers were prepared on two different substrates: Si_3N_4 and SiO_2 , resulting in strong covalent C–N/C–Si and C–O–Si interfacial bonds, respectively. Additionally, 2-[[methoxy-oligo-(EO)_{6–9}]-propyl]trimethoxysilane on glass provided the mixed monolayer $M_{SiO_2}^2$, containing oligo-EO tails with six to nine EO units.

The monolayers were studied in positive-ion mode by analyzing several adjacently positioned samples in one run (Figure 3). For all oligo(EO)-terminated monolayers, we observed C–O scission at different positions in the EO tail and subsequent formation of two homologous series of protonated fragments. The first series was composed of truncated oligomers with methoxy/carbonyl chain ends, $[CH_3O-(CH_2CH_2O)_nCH_2CHO + H]^+$ (Figure 2; marked as a_n), while the second series had methoxy/hydroxyl chain ends $[CH_3O(CH_2CH_2O)_nCH_2CH_2OH + H]^+$ (Figure 3, marked as b_n). The m/z of the observed ions was directly related to the length of the EO chain. The reconstructed ion chromatogram of $M_{SiO_2}^{EO3}$, for instance, demonstrated peaks of relatively high abundance but only with $n = 1–2$ (data not shown). Likewise, monolayers with six EO units, for example, $M_{SiO_2}^{EO6}$ and $M_{Si_3N_4}^{EO6}$, gave rise to the oligomers with $n = 1–5$, while monolayers with nine EO units, for example, $M_{SiO_2}^{EO9}$ and $M_{Si_3N_4}^{EO9}$, produced not only the aforementioned oligomers but also longer fragments ($n = 1–8$). Thus, by DART-HRMS analysis, it is possible to break down the EO chain unit by unit, and to determine the longest oligo-EO linker present on the surface. Consequently in the case of the mixed monolayer $M_{SiO_2}^2$, all fragments with n between 1 and 8 were found. Apart from the said oligomers, their corresponding NH_4^+ -cationized species were also detected but with lower abundance.

DART-HRMS of Poly(Ethylene Glycol)-Terminated Layers. Having shown that short monolayers with ether bonds can be analyzed by DART-HRMS, the question arose whether analysis of high-molecular weight polyether layers was also feasible. To this aim, the reactive ester-terminated monolayer M_{Au}^2 was used for the covalent attachment of a bifunctional poly(ethylene glycol) (PEG) with NH_2 and $COOH$ as terminal groups. The attachment thus proceeded via amide bond formation on the surface. In this fashion two different PEGs were attached, mainly a 22-mer (PEG, 1 kDa),

yielding the carboxymethyl-PEG-terminated layer M_{Au}^3 , and a 77-mer (PEG, 3.5 kDa) for obtaining the carboxymethyl-PEG-terminated layer M_{Au}^4 . The DART-HRMS analysis of these layers in positive-ion mode, showed series of homologous fragments each differing 44.0260 (C_2H_4O) following C–O and C–C scission of the polymer chain.⁴³ In contrast to the oligo-EO monolayers discussed above, all these ions were NH_4^+ adducts, and the most intense ions were assigned to truncated fragments bearing the carboxymethyl chain end of the polymer: $[HOOC - CH_2O(CH_2CH_2O)_nCH_2CHO + NH_4]^+$ (Figure 3d). The highest MW fragment observed for these monolayers was the 12-mer because ions with higher mass and higher polarity most probably cannot be desorbed by DART. Ions bearing the amino chain end of the polymers were clearly discerned only in solution, while on the surface after amide bond formation and covalent attachment, ions with the free amino chain end of the polymer were not observed in positive-ion mode of DART. Measurement of M_{Au}^3 in positive-ion mode showed that not all of the original PFP groups of M_{Au}^2 had reacted with the amino-terminated PEG (Figure 3d insert). This could be more sensitively confirmed by scanning the same surfaces in negative-ion mode (PFP anion). This shows that DART-HRMS can be used in a semiquantitative fashion to follow monolayer synthesis.

DART-HRMS of Sugar-Terminated Monolayers. The potential of DART-HRMS to analyze thermally labile biomolecules attached on a surface was evaluated with lactose, mannose and fucose-functionalized monolayers on Al_2O_3 : $M_{Al_2O_3}^{lac}$, $M_{Al_2O_3}^{man}$, and $M_{Al_2O_3}^{fuc}$. Sugar-terminated monolayers find wide applications in biosensors,⁴⁴ molecular diagnostics,³³ and drug delivery.⁴⁵ The DART-HRMS analysis of these specimens in positive-ion mode did not show ions related to the original azidoundecanyl carbohydrates **1**, **4**, or **7** (see SI) used in their synthesis confirming XPS analyses. Given the previously observed efficient cleavage of ether linkages in e.g. oligo-ethylene oxide monolayers, we expected C–O bond cleavage and ions for the corresponding monosaccharides. Indeed, these ions were detected, which implies C–O scission and ionization of the carbohydrate fragments. On monolayers $M_{Al_2O_3}^{man}$ and $M_{Al_2O_3}^{lac}$, for example, several adducts, described previously as being characteristic for a monosaccharide in solution $C_6H_{12}O_6$,^{46,47} were identified: $[C_6H_{12}O_6 + NH_4]^+$ at m/z 198.0969, $[C_6H_{12}O_6 + NH_4 - H_2O]^+$ at m/z 180.0863, $[C_6H_{12}O_6 + NH_4 - H_2O - NH_3]^+$ at m/z 163.0597, and $[C_6H_{12}O_6 + NH_4 - 2H_2O - NH_3]^+$ at m/z 145.0492. In addition to the aforementioned ions, on monolayer $M_{Al_2O_3}^{lac}$ ions related to a disaccharide $C_{12}H_{22}O_{11}$ were found: $[C_{12}H_{22}O_{11} + NH_4 - NH_3]^+$ at m/z 343.1229 and $[C_{12}H_{22}O_{11} + NH_4 - H_2O]^+$ at m/z 342.1387 (see mass spectral library, SI). The latter ion but not the former ion was reported by Wang et al. in their recent DART-MS study on dissolved sugars.⁴⁷ Instead they reported an $[M + NH_4]^+$ for lactose, which was not observed in our surface analysis. Similarly the fucose-terminated monolayer $M_{Al_2O_3}^{fuc}$ demonstrated two ions for fucose $C_6H_{12}O_5$, namely $[C_6H_{12}O_5 + NH_4 - H_2O]^+$ at m/z 164.0915 and $[C_6H_{12}O_5 + NH_4 - 2H_2O - NH_3]^+$ at m/z 147.0649. Thus, DART-HRMS has the ability to discriminate between covalently immobilized monosaccharides and disaccharides, that is, it could play a role in surface MS analysis of carbohydrate-based biosensors. It also shows that even

Table 2. Summary of Characteristic Ions of Monolayers Observed with DART-HRMS

Monolayer type	Characteristic ions observed in DART-HRMS	
	positive-ion mode	negative-ion mode
R-(C=O)O-surface	none	[R-(C=O)O] [−]
R-O(C=O)-surface	none	[RO] [−]
R-(C=O)NH-surface	none	[R-(C=O)O] [−]
R-NH(C=O)-surface	[R-NH ₂ + H] ⁺	none
CH ₃ (CH ₂) ₉ S-Au	[M + 2O - H] ⁺ , [M + O - 3H] ⁺ , [M + O - H] ⁺ , [M + 3O - H] ⁺ , [M + 2O - 3H] ⁺ , [2M - SH + 2O] ⁺ , [2M - SH + 2O - H ₂ O] ⁺ , [2M - SH + 4O - H] ⁺ , M is CH ₃ (CH ₂) ₉ SH	[CH ₃ (CH ₂) ₉ SO ₃] [−] , [CH ₃ (CH ₂) ₉ SO ₂] [−]
HOOC-(CH ₂) ₁₅ -S-Au	[HOOC-(CH ₂) ₁₅ -S] ⁺ , loss of H ₂ and H ₂ S	not measured
R-S-C _x H _y -surface	none	[RSO ₃] [−] , [RSO ₂] [−]
C _x H _y -surface	none	none
CH ₃ O(EO) _n (CH ₂) _x -surface	[CH ₃ O(EO) _n CH ₂ CHO + H] ⁺ , [CH ₃ O(EO) _n CH ₂ CH ₂ OH + H] ⁺	none
HOOC-CH ₂ PEG-surface	[HOOCCH ₂ O(CH ₂ CH ₂ O) _n CH ₂ CHO + NH ₄] ⁺	none
monosaccharide-surface	[C ₆ H ₁₂ O ₆ + NH ₄] ⁺ , [C ₆ H ₁₂ O ₆ + NH ₄ - H ₂ O] ⁺ , [C ₆ H ₁₂ O ₆ + NH ₄ - H ₂ O - NH ₃] ⁺ , [C ₆ H ₁₂ O ₆ + NH ₄ - 2H ₂ O - NH ₃] ⁺	not measured
disaccharide-surface	[C ₆ H ₁₂ O ₆ + NH ₄] ⁺ , [C ₆ H ₁₂ O ₆ + NH ₄ - H ₂ O] ⁺ , [C ₆ H ₁₂ O ₆ + NH ₄ - H ₂ O - NH ₃] ⁺ , [C ₆ H ₁₂ O ₆ + NH ₄ - 2H ₂ O - NH ₃] ⁺ , [C ₁₂ H ₂₂ O ₁₁ + NH ₄ - NH ₃] ⁺ , [C ₁₂ H ₂₂ O ₁₁ + NH ₄ - H ₂ O] ⁺	not measured

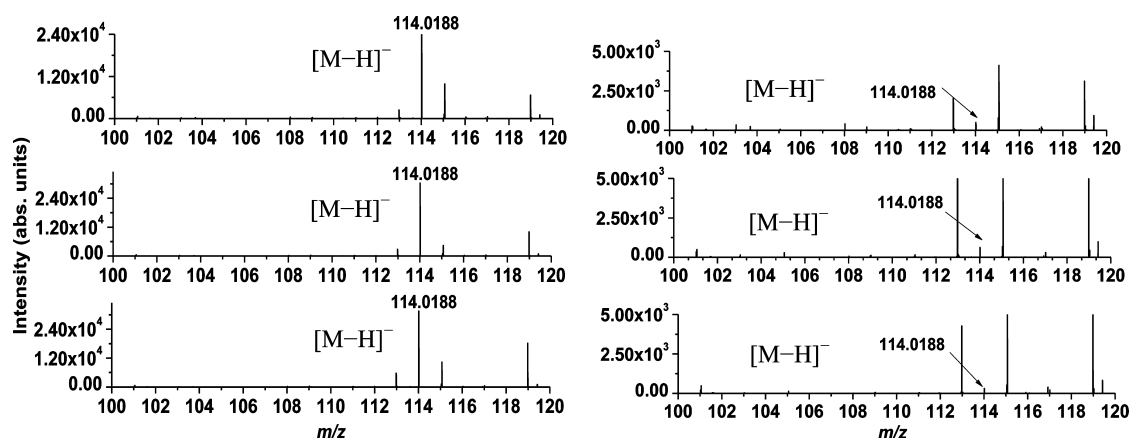


Figure 4. Negative-ion mode DART-HRMS of two types of commercial NHS glass slides. Left: 3 measurements of one slide of PolyAn. Right: 3 measurements of one slide of Schott. Please note difference in vertical axis values. The ions observed at m/z 113, 115, and 119 are due to background.

monolayers incorporating very polar, nonvolatile, thermally labile molecules, are amenable to analysis by DART-HRMS.

Application to Commercially Available Samples. On the basis of all collected mass spectra of in-house prepared monolayers, specific ions characteristic for these monolayers were summarized in Table 2. Using this table, the surface chemistry of unknown samples can be easily evaluated. To demonstrate this for quality control of commercially available surfaces, several glass slides for microarrays (PolyAn GmbH and Schott) and gold SPR chips (XanTec biondiagnostics) with different covalently attached monolayers (syn. coatings) were analyzed. Such engineered surfaces, used for bioassays and diagnostic purposes, are often supplied with limited information about the surface chemistry present. Therefore, a fast and reliable surface analysis tool could provide proper characterization and aid in the manufacturing process.

SPR chips (XanTec biondiagnostics) with the coating CMPGx are stated to be modified gold surfaces with a carboxymethyl-PEG (6 kDa) thin film. According to the manufacturer, this coating is suitable for further attachment of NH₂-terminated compounds, suggesting that the COOH terminal groups are free and available on the surface for further functionalization. Carboxymethyl-PEG coatings are best analyzed with DART-HRMS in positive-ion mode, and truncated fragments from homologous series [HOOC - CH₂O(CH₂CH₂O)_nCH₂CHO

+ NH₄]⁺ were expected (Table 2). In the positive-ion mass spectra of the SPR chip with CMPGx chip coating, the aforementioned set of ions were clearly observed, which confirmed the presence of terminal carboxymethyl-PEG groups. However, their intensity was 1 order of magnitude lower than that of the same ions detected in M_{Au}³⁺ and M_{Au}⁴⁺ (Figure S20, SI). This could be due to a lower surface coverage of carboxymethyl-PEG terminal groups on the SPR chip. This hypothesis is supported by the fact that fragments from this set of ions were detected only with n between 2 and 7, while ions with higher m/z values, as big as 12-mer could be detected from the in-house prepared monolayers.

Additionally, microarray glass slides with PEG coating (PolyAn) were also analyzed with DART-HRMS. On these PEG-ylated slides, very intense ions were observed differing by 44.0256 Da (C₂H₄O). In the mass spectrum, two homologous series of fragments could be clearly discerned: [C₈H₁₈O₄ - (PEG)_n + NH₄]⁺ and [C₆H₁₀O₃ - (PEG)_n + H]⁺.

Furthermore, PolyAn's microarray glass slides with terminal ester groups, namely, *N*-hydroxysuccinimide (NHS), were also probed with DART-HRMS. The ester terminated glass slides were analyzed in negative-ion mode³⁴ (Table 2), and the presence of intense peaks at m/z 114.0188 for [M - H][−] (Figure 4 left) and at m/z 229.0454 for [2M - H][−] (not shown), where M is NHS alcohol, confirmed the claimed

surface functionality. In order to check on-slide reproducibility and batch-to-batch reproducibility of PolyAn's NHS (Figure 4 left) and PEG slides, three specimens from one slide and two slides taken from two different batches (5 slides per batch) were subjected to DART-HRMS. The results were consistent and demonstrated good on-slide reproducibility and batch-to-batch reproducibility for both types of chemistries.

Glass slides with NHS terminal groups from another supplier (Schott) were also analyzed (Figure 4 right). However, in this case the signal at m/z 114.0188 for $[M - H]^-$, where M is the NHS alcohol, was 2 orders of magnitude lower than for the PolyAn slides, and the ion for $[2M - H]^-$ was not detected at all. Additionally, the signal intensity of m/z 114.0187 varied (RSDs for PolyAn and Schott slides were 9% and 107%, respectively) and suggested within-slide irreproducibility (Figure 4 right). This evidently shows the usefulness of DART-HRMS for quality control of monolayers.

CONCLUSIONS

In 2009, Richman and Hutchison in their paper "The Nanomaterial Characterization Bottleneck" wrote "To reap the benefits of nanotechnology, improvements in characterization are needed to increase throughput as creativity outpaces our ability to confirm results".² Current surface analysis tools, such as SEM, fluorescence, and XPS cannot provide sufficiently detailed molecular information about the monolayer present. SIMS and MALDI-MS to some extent can but not under ambient conditions, and they suffer from fragmentation and background problems, respectively. Here we have shown, through a detailed analysis of a wide range of organic monolayers on five different substrates, that DART-HRMS is able to provide such detailed chemical information for most monolayers. It does so in a simple, rapid, sensitive and reproducible manner under ambient conditions without any sample preparation and the fragmentation is in most cases predictable (Table 2). Thus DART-HRMS displays all the ingredients to become a valuable complementary tool in the analysis of nm-thick layers leading to better characterization and thus removing bottlenecks on the way to improved engineered surfaces. Already we have shown that DART-MS is able to detect semiquantitatively differences in the density of active groups of commercial nm-thick coatings. To facilitate further studies of organically modified surfaces by DART-HRMS, relevant spectra of all surfaces were compiled in a mass spectral library, which is freely available in the Supporting Information.

ASSOCIATED CONTENT

Supporting Information

Experimental details, XPS, NMR, movie of actual measurement of surface, and mass spectra. This material is available free of charge via the Internet at <http://pubs.acs.org>.

AUTHOR INFORMATION

Corresponding Author

*E-mail: teris.vanbeek@wur.nl. Phone: (+31) 317-482376. Fax: (+31) 317-484914.

Notes

The authors declare no competing financial interest.

ACKNOWLEDGMENTS

The authors thanks the INTERREG IV A Germany–Netherlands program, the European Regional Development Fund, the MWEBWV Ministry of North-Rhine Westphalia, the Dutch Ministry of Economic Affairs, Province of Gelderland, and the program management Euregio Rhein-Waal for funding this project.

REFERENCES

- (1) European Commission. Commission Staff Working Paper, 2012. <http://go.nature.com/Hebkwm>.
- (2) Richman, E. K.; Hutchison, J. E. *ACS Nano* **2009**, *3*, 2441–2446.
- (3) Yu, T.; Greish, K.; McGill, L. D.; Ray, A.; Ghandehari, H. *ACS Nano* **2012**, *6*, 2289–2301. Riehemann, K. *Small* **2012**, *8*, 1970–1972.
- (4) Schürs, F.; Lison, D. *Nat. Nanotechnol.* **2012**, *7*, 546–548. Krug, H. F.; Wick, P. *Angew. Chem., Int. Ed.* **2011**, *50*, 1260–1278.
- (5) Yang, W.; Zhang, R.; Willett, G. D.; Hibbert, D. B.; Gooding, J. J. *Anal. Chem.* **2003**, *75*, 6741–6744.
- (6) Hanley, L.; Kornienko, O.; Ada, E. T.; Fuoco, E.; Trevor, J. L. *J. Mass Spectrom.* **1999**, *34*, 705–723.
- (7) Zelzer, M.; McNamara, L. E.; Scurr, D. J.; Alexander, M. R.; Dalby, M. J.; Ulijn, R. V. *J. Mater. Chem.* **2012**, *22*, 12229–12237.
- (8) Urquhart, A. J.; Taylor, M.; Anderson, D. G.; Langer, R.; Davies, M. C.; Alexander, M. R. *Anal. Chem.* **2007**, *80*, 135–142.
- (9) Hutt, D. A.; Cooper, E.; Leggett, G. J. *J. Phys. Chem. B* **1998**, *102*, 174–184.
- (10) Trevor, J. L.; Mencer, D. E.; Lykke, K. R.; Pellin, M. J.; Hanley, L. *Anal. Chem.* **1997**, *69*, 4331–4338.
- (11) Laiho, T.; Leiro, J. A. *Surf. Interface Anal.* **2008**, *40*, 51–59.
- (12) Offord, D. A.; John, C. M.; Griffin, J. H. *Langmuir* **1994**, *10*, 761–766.
- (13) Li, Y.; Huang, J.; McIver, R. T.; Hemminger, J. C. *J. Am. Chem. Soc.* **1992**, *114*, 2428–2432.
- (14) Shibue, T.; Nakanishi, T.; Matsuda, T.; Asahi, T.; Osaka, T. *Langmuir* **2002**, *18*, 1528–1534.
- (15) Trevor, J. L.; Lykke, K. R.; Pellin, M. J.; Hanley, L. *Langmuir* **1998**, *14*, 1664–1673.
- (16) Yan, B.; Zhu, Z.-J.; Miranda, O.; Chomposor, A.; Rotello, V.; Vachet, R. *Anal. Bioanal. Chem.* **2010**, *396*, 1025–1035.
- (17) Zhu, Z.-J.; Tang, R.; Yeh, Y.-C.; Miranda, O. R.; Rotello, V. M.; Vachet, R. W. *Anal. Chem.* **2012**, *84*, 4321–4326.
- (18) Su, J.; Mrksich, M. *Langmuir* **2003**, *19*, 4867–4870.
- (19) Dass, A.; Stevenson, A.; Dubay, G. R.; Tracy, J. B.; Murray, R. W. *J. Am. Chem. Soc.* **2008**, *130*, 5940–5946. Kim, B. H.; Shin, K.; Kwon, S. G.; Jang, Y.; Lee, H.-S.; Lee, H.; Jun, S. W.; Lee, J.; Han, S. Y.; Yim, Y.-H.; Kim, D.-H.; Hyeon, T. *J. Am. Chem. Soc.* **2013**, *135*, 2407–2410.
- (20) Roth, M.; Kim, J.; Maresh, E.; Plymire, D.; Corbett, J.; Zhang, J.; Patrie, S. J. *Am. Soc. Mass Spectrom.* **2012**, *23*, 1661–1669.
- (21) Gurard-Levin, Z. A.; Mrksich, M. *Annu. Rev. Anal. Chem.* **2008**, *1*, 767–800.
- (22) Mrksich, M. *ACS Nano* **2008**, *2*, 7–18.
- (23) Li, S.; Liao, X.; Mrksich, M. *Langmuir* **2012**, *29*, 294–298.
- (24) Patrie, S. M.; Mrksich, M. *Anal. Chem.* **2007**, *79*, S878–S887.
- (25) Ban, L.; Pettit, N.; Li, L.; Stuparu, A. D.; Cai, L.; Chen, W.; Guan, W.; Han, W.; Wang, P. G.; Mrksich, M. *Nat. Chem. Biol.* **2012**, *8*, 769–773.
- (26) Montavon, T. J.; Li, J.; Cabrera-Pardo, J. R.; Mrksich, M.; Kozmin, S. A. *Nat. Chem.* **2012**, *4*, 45–51.
- (27) Ocsay, I.; Gulbakan, B.; Shukoor, M. I.; Xiong, X.; Chen, T.; Powell, D. H.; Tan, W. *ACS Nano* **2012**, *7*, 417–427.
- (28) Monge, M. E.; Harris, G. A.; Dwivedi, P.; Fernández, F. M. *Chem. Rev.* **2013**, *113*, 2269–2308.
- (29) Kpegba, K.; Spadaro, T.; Cody, R. B.; Nesnas, N.; Olson, J. A. *Anal. Chem.* **2007**, *79*, 5479–5483.
- (30) Ma, L.; Jia, M.; Hu, J.; Ouyang, J.; Na, N. *J. Am. Soc. Mass Spectrom.* **2012**, *23*, 1271–1278.

- (30) (a) Onclin, S.; Ravoo, B. J.; Reinhoudt, D. N. *Angew. Chem., Int. Ed.* **2005**, *44*, 6282–6304. (b) ter Maat, J.; Regeling, R.; Yang, M.; Mullings, M. N.; Bent, S. F.; Zuilhof, H. *Langmuir* **2009**, *25*, 11592–11597.
- (31) Rosso, M.; Giesbers, M.; Arafat, A.; Schroën, K.; Zuilhof, H. *Langmuir* **2009**, *25*, 2172–2180.
- (32) (a) Li, Y.; Calder, S.; Yaffe, O.; Cahen, D.; Haick, H.; Kronik, L.; Zuilhof, H. *Langmuir* **2012**, *28*, 9920–9929. (b) Ciampi, S.; Harper, J. B.; Gooding, J. J. *Chem. Soc. Rev.* **2010**, *39*, 2158–2183.
- (33) ter Maat, J.; Regeling, R.; Ingham, C. J.; Weijers, C. A. G. M.; Giesbers, M.; de Vos, W. M.; Zuilhof, H. *Langmuir* **2011**, *27*, 13606–13617.
- (34) Manova, R. K.; Claassen, F. W.; Nielen, M. W. F.; Zuilhof, H.; van Beek, T. A. *Chem. Commun.* **2013**, *49*, 922–924.
- (35) Manova, R. K.; Pujari, S. P.; Weijers, C. A. G. M.; Zuilhof, H.; van Beek, T. A. *Langmuir* **2012**, *28*, 8651–8663.
- (36) Cody, R. B. *Anal. Chem.* **2008**, *81*, 1101–1107.
- (37) Tarlov, M. J.; Newman, J. G. *Langmuir* **1992**, *8*, 1398–1405.
- (38) Wong, S. C. C.; Lockyer, N. P.; Vickerman, J. C. *Surf. Interface Anal.* **2005**, *37*, 721–730.
- (39) Bhairamadgi, N. S.; Gangarapu, S.; Caipa Campos, M. A.; Paulusse, J. M. J.; van Rijn, C. J. M.; Zuilhof, H. *Langmuir* **2013**, *29*, 4535–4542.
- (40) Cody, R.; Dane, A. J. *J. Am. Soc. Mass Spectrom.* **2013**, 329–334.
- (41) Yang, L.; Lua, Y.-Y.; Jiang, G.; Tyler, B. J.; Linford, M. R. *Anal. Chem.* **2005**, *77*, 4654–4661.
- (42) Amalric, J.; Poleunis, C.; Delcorte, A.; Marchand-Brynaert, J. *Surf. Sci.* **2012**, *606*, 1071–1077.
- (43) Wesdemiotis, C.; Solak, N.; Polce, M. J.; Dabney, D. E.; Chaicharoen, K.; Katzenmeyer, B. C. *Mass Spectrom. Rev.* **2011**, *30*, 523–559.
- (44) Cunningham, S.; Gerlach, J. Q.; Kane, M.; Joshi, L. *Analyst* **2010**, *135*, 2471–2480.
- (45) Gorityala, B. K.; Lu, Z.; Leow, M. L.; Ma, J.; Liu, X.-W. *J. Am. Chem. Soc.* **2012**, *134*, 15229–15232.
- (46) Saang’onyo, D. S.; Smith, D. L. *Rapid Commun. Mass Spectrom.* **2012**, *26*, 385–391.
- (47) Wang, Y.; Liu, L.; Ma, L.; Liu, S. *Int. J. Mass. Spectrom.* **2014**, *357*, 51–57.